Energy Conversion and Management 86 (2014) 1173–1185

Contents lists available at ScienceDirect

Energy Conversion and Management

journal homepage: www.elsevier.com/locate/enconman

# A biogeography-based optimization algorithm with mutation strategies for model parameter estimation of solar and fuel cells

Qun Niu [a,*], Letian Zhang [a], Kang Li [b]

[a] School of Mechatronic Engineering and Automation, Shanghai Key Laboratory of Power Station Automation Technology, Shanghai University, Shanghai 200072, China
[b] Energy, Power and Intelligent Control, School of Electronics, Electrical Engineering and Computer Science, Queen's University Belfast, Belfast BT9 5AH, UK

ARTICLE INFO

*Article history:*
Received 3 January 2014
Accepted 10 June 2014

*Keywords:*
Solar cell
PEM fuel cell
Biogeography-based optimization
Mutation strategy
Parameter estimation

ABSTRACT

Mathematical models are useful tools for simulation, evaluation, optimal operation and control of solar cells and proton exchange membrane fuel cells (PEMFCs). To identify the model parameters of these two type of cells efficiently, a biogeography-based optimization algorithm with mutation strategies (BBO-M) is proposed. The BBO-M uses the structure of biogeography-based optimization algorithm (BBO), and both the mutation motivated from the differential evolution (DE) algorithm and the chaos theory are incorporated into the BBO structure for improving the global searching capability of the algorithm. Numerical experiments have been conducted on ten benchmark functions with 50 dimensions, and the results show that BBO-M can produce solutions of high quality and has fast convergence rate. Then, the proposed BBO-M is applied to the model parameter estimation of the two type of cells. The experimental results clearly demonstrate the power of the proposed BBO-M in estimating model parameters of both solar and fuel cells.


## 1. Introduction

The greenhouse emissions and fossil fuels shortage are the twin challenges facing the mankind, and the development of new clean energy technologies has been recognized as the key to tackle the problems. Solar cells and proton exchange membrane fuel cells (PEMFCs) have attracted considerable attention due to the features of their high power density, no pollution and low noise. As photoelectric converters, solar cells not only have no byproduct but also have the advantages of easy installation and little maintenance cost. Similarly, PEMFCs generate electricity by oxidizing hydrogen under relative low operating temperatures with non-polluting byproducts, and have been widely used in vehicle propulsion, small distributed generation and portable applications [1–4].

Modeling the operation of solar cells and PEMFCs has become a significant research topic in recent years in order to better explore and utilize their properties. Some models have been proposed to simulate the behaviors of both cells under different operating conditions [5–10], and most of them are less useful in practical applications due to the complexity and problem specific. In recent years, mathematical models with some unknown parameters are widely used in practice [11–13]. These parameters which reflect the actual performances (such as air pressure, fuel flow rate, cell temperature, diffusion and recombination diode resistance) are primarily chosen based on experience, and these low-accurate empirical values inevitably affect effectiveness of the developed models in simulation, design, optimal operation and control. Therefore, it is indispensable to investigate the problems of parameter estimation problems of the solar cell and PEMFC models.

Some conventional deterministic optimization methods have been used to solve the parameter estimations [14–18]. However, these two kinds of cells are nonlinear, non-convex and strongly coupled systems and most of these conventional approaches require continuity, convexity and differentiability conditions, which make them hard to handle the parameter estimation problems mentioned above. With the development of computing technologies and artificial intelligence, many meta-heuristic optimization algorithms, which are of conceptual and computational simplicity, being excellent real-world problem solvers and robust to dynamic environments, capable of solving problems with no known solutions and with no need for analytic expression of the problems [19], have been applied to the parameter estimation problems of solar cell and PEMFC. Genetic algorithm (GA) [20–23], simulated annealing (SA) [24,25], particle swarm optimization (PSO) [26–29], differential evolution (DE) [30,31] and artificial neural networks (ANNs) [32,33] have been proposed to improve the parameter accuracy for both cell models respectively. Besides, several other methods including bird mating optimizer (BMO) [34,35] and seeker optimization algorithm (SOA) [36] have also been used to solve

* Corresponding author. Tel.: +86 021 56334241; fax: +86 021 56334241.
*E-mail address:* comelycc@hotmail.com (Q. Niu).

http://dx.doi.org/10.1016/j.enconman.2014.06.026
0196-8904/

**Nomenclature**

| | |
|---|---|
| $V_C$ | the output voltage (V) |
| $T$ | temperature in Kelvin (K) |
| *Solar cell* | |
| $I_C$ | output current (A) |
| $I_{ph}$ | photo-induced current (A) |
| $I_{D1}$, $I_{D2}$, $I_D$ | diode current (A) |
| $I_{SD1}$, $I_{SD2}$ | saturation current (A) |
| $I_{sh}$ | shunt resistor current (A) |
| $R_S$ | series resistance (Ω) |
| $R_{SH}$ | shunt resistance (Ω) |
| $n$, $n_1$, $n_2$ | diode ideality constants |
| $q$ | electronic charge (C) |
| $k$ | Boltzmann constant (J/K) |
| *PEM fuel cell* | |
| $E_{Nernst}$ | reversible open circuit voltage (V) |
| $V_{act}$ | activation voltage loss (V) |
| $V_{ohmic}$ | ohmic voltage loss (V) |
| $V_{con}$ | concentration voltage loss (V) |
| $P_{O_2}$ | partial pressure of the oxygen (atm) |
| $P_{H_2}$ | partial pressure of the hydrogen (atm) |
| $P^{sat}_{H_2O}$ | saturation pressure of water (atm) |
| $P_a$ | inlet anode pressure (atm) |
| $P_c$ | inlet cathode pressure (atm) |
| $RH_a$ | relative humidity in anode |
| $RH_c$ | relative humidity in cathode |
| $i$ | experimental current (A) |
| $\xi_1$, $\xi_2$, $\xi_3$, $\xi_4$ | parametric coefficient of cell |
| $C_{O_2}$ | oxygen concentration (mol/cm$^3$) |
| $R_M$ | membrane resistance (Ω) |
| $R_C$ | contact resistance ($\Omega$) |
| $\rho_M$ | membrane specific resistivity (Ω/cm) |
| $l$ | membrane thickness (cm) |
| $\lambda$ | parameter influenced by anode gas |
| $b$ | concentration loss constant (V) |
| $I_{max}$ | maximum current density (A/cm$^2$) |
| $N_s$ | number of series PEM fuel cells |
| $A$ | efficient active area of cell (cm$^2$) |

the PEMFC model parameter estimation problem. In addition, the solar cell modeling problem was addressed by pattern search (PS) [37] and artificial bee swarm optimization algorithm (ABSO) [38]. Although these methods have achieved good performance, they are only used for single cell parameter estimation and potentially do not fit other cell problems, and parameter estimation is a challenging problem which requires the obtained physical parameters match well with reality. It is necessary to find a new approach to solve both solar cell and PEMFC problems more efficiently.

Biogeography-based optimization (BBO) proposed by Dan Simon in 2008 [39] is a stochastic global search technique which attempts to imitate the phenomenon of the theory of island biogeography, and it has two operators namely migration and mutation. Although the BBO has been applied to a number of real world optimization problems such as chemical industry [42], power systems [43], control systems [44] and scheduling problems [45], to the best of our knowledge, no studies have been reported so far on applying the BBO method to the parameter estimation problems of fuel and solar cells. In this paper, the BBO algorithm with two mutation strategies (BBO-M) is proposed to identify the optimal estimation parameters of both solar cell and PEMFC models. Considering about some drawbacks of conventional BBO [46], two improvements are designed to combine with BBO. In order to enhance the exploitation, the mutation strategy from differential evolution (DE) is introduced into the migration of BBO in this paper. Meanwhile, to avoid premature convergence, chaos theory [47] is also employed in BBO to adjust the solution in the mutation stage. To demonstrate the performance of the BBO-M method, it is compared with conventional BBO and four popular methods, including DE [48], GHS [49], PSO-w [50], GA toolbox [51] on ten numerical benchmark functions. Furthermore, BBO-M is also employed to estimate the parameters of both solar cell and PEMFC problems and compared with the reported results in the literatures. According to the results obtained, the BBO-M shows a superior performance and the potential in solving real-life problems.

## 2. Electrochemical models for the solar cell and fuel cell

### 2.1. Solar cell models

A solar cell is a conversion device that converts the light energy to electrical energy directly and continuously. Among various types of solar cell models, only two are widely used. The first one is the double diode model which incorporates an additional and separate current diode with its own exponential voltage dependence [11]. The second model, commonly known as the single diode model, assumes that one lumped diode mechanism is enough to describe the characteristic of the solar cell [12]. In the following subsections these two models will be given.

#### 2.1.1. Double diode model

The double diode model is shown in Fig. 1, which conforms quite closely to the Shockley theory [52]. When exposed to the light, the solar cell will absorb the photons and create an electron–hole pair in the case that the energy of the photons is higher than the band gap energy of the semiconductor, and the output current of the model can be calculated as follows:

$$I_C = I_{ph} - I_{D1} - I_{D2} - I_{sh} \tag{1}$$

where $I_C$ denotes the output current, $I_{ph}$ is the photo-induced current, $I_{D1}, I_{D2}$ are the first and second diode currents, and $I_{sh}$ denotes the shunt resistor current. The two diodes currents $I_{D1}$ and $I_{D2}$ are formulated respectively in Eqs. (1) and (2), and the shunt resistor current $I_{sh}$ is illustrated in Eq. (4):

$$I_{D1} = I_{SD1}\left[\exp\left(\frac{q(V_C + I_C R_S)}{n_1 kT}\right) - 1\right] \tag{2}$$

$$I_{D2} = I_{SD2}\left[\exp\left(\frac{q(V_C + I_C R_S)}{n_2 kT}\right) - 1\right] \tag{3}$$

$$I_{sh} = \frac{V_C + I_C R_S}{R_{sh}} \tag{4}$$

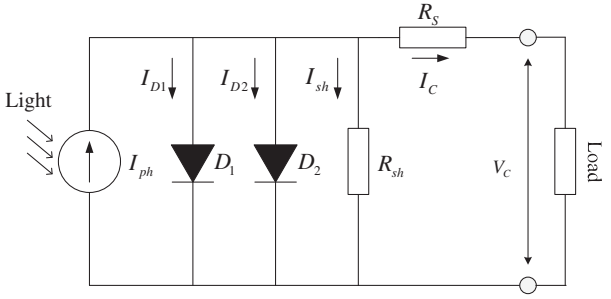


**Fig. 1.** The double diode model of the solar cell.

where $V_C$ is the output voltage, $R_S$ is the series resistance which provides a more accurate shape between the maximum power point and the open circuit voltage, $R_{sh}$ is the shunt resistance that parallels the diodes, $I_{SD1}$ is the saturation current due to diffusion mechanism, $I_{SD2}$ describes the saturation current due to recombination in space-charge layer, $q$ is the electronic charge (1.60217646e−19 $C$), $k$ is the Boltzmann constant (1.3806503e−23 $J/K$), $n_1$ and $n_2$ are defined as the diffusion and recombination diode ideality constants, and T is the temperature of the solar cell in Kelvin (306.15 $K$) [14].

From Eqs. (1)–(4), it is shown that the double diode model of the solar cell has seven unknown parameters $(R_S, R_{sh}, I_{ph}, I_{D1}, I_{SD2}, n_1, n_2)$ which need to be identified.

### 2.1.2. Single diode model

Fig. 2 illustrates the single diode model, which is a simplified version of the double diode model. The single diode model is in fact a sub-circuit of the double one and has been widely used to describe the $I$–$V$ characteristics of the solar cells [53]. The current–voltage relationship of the single diode model can be described as:

$$I_C = I_{ph} - I_D - I_{sh} \tag{5}$$

$$I_D = I_{SD}\left[\exp\left(\frac{q(V_C + I_C R_S)}{nkT}\right) - 1\right] \tag{6}$$

$$I_{sh} = \frac{V_C + I_C R_S}{R_{sh}} \tag{7}$$

In this single diode model, the number of unknown parameters is reduced to five which are $R_S, R_{sh}, I_{ph}, I_{SD}, n$.

### 2.1.3. Objective function

In the parameter estimation problem, the main objective is to minimize the error between measured and simulated current. In this paper, the objective function $F_{sc}$ is described as the root mean square of the error between the simulated and experimental current data. It is given as follows:

$$F_{sc} = \sqrt{\frac{1}{N}\sum_{i=1}^{N}(f(V_i, I_i, x) - I_i)^2} \tag{8}$$

where $N$ is the number of the solar cell experimental data. $V_i$ and $I_i$ are the $i$th experimental voltage and current respectively. $f(V_i, I_i, x)$ is the simulated current data,which can be calculated using Eqs. (9) and (10).

$$\begin{aligned} f(V_i, I_i, x) &= I_{ph} - I_{D1} - I_{D2} - I_{sh} \\ &= I_{ph} - I_{SD1}\left[\exp\left(\frac{q(V_i + I_i R_S)}{n_1 kT}\right) - 1\right] \\ &\quad - I_{SD2}\left[\exp\left(\frac{q(V_i + I_i R_S)}{n_2 kT}\right) - 1\right] - \frac{V_i + I_i R_S}{R_{sh}} \end{aligned} \tag{9}$$

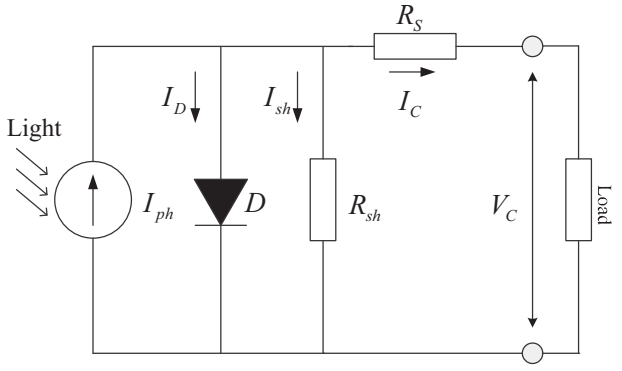


**Fig. 2.** The single diode model of the solar cell.

$$\begin{aligned} f(V_i, I_i, x) &= I_{ph} - I_D - I_{sh} \\ &= I_{ph} - I_{SD}\left[\exp\left(\frac{q(V_i + I_i R_S)}{nkT}\right) - 1\right] - \frac{V_i + I_i R_S}{R_{sh}} \end{aligned} \tag{10}$$

In Eq. (9), $x = (R_S, R_{sh}, I_{ph}, I_{D1}, I_{SD2}, n_1, n_2)$ are the seven parameters of the double diode solar cell model to be identified, and in Eq. (10), $x = (R_S, R_{sh}, I_{ph}, I_{SD}, n)$ are the five parameters of the single diode solar cell model to be identified. The upper and lower limits for these parameters are taken from the literatures [14–16,18], and are listed in Table 1. It is obvious that the smaller the error between the measured and simulated current data, the more accurate the model is.

## 2.2. PEM fuel cell

The proton exchange membrane fuel cell (PEMFC) transforms the chemical energy liberated during the electrochemical reaction of hydrogen and oxygen to electrical energy, as opposed to the direct combustion of hydrogen and oxygen gases to produce thermal energy. Fig. 3 shows the major components of a generic PEMFC system, including sealed fuel cell stack, fuel supply, electrolyte, water management and humidifier. Hydrogen and oxygen must be humidified before they are supplied into the fuel cell. The hydrogen gas is transferred to the anode through a narrow channel, and is oxidized into hydrogen ions and electrons. The hydrogen ions pass through the electrolyte (proton exchange membrane) to the cathode. The electrons reach the cathode through the exterior circuit and generate the current. When the hydrogen ions and electrons combine with the oxygen in the cathode, they react to produce water and release the energy in form of heat. The electrochemical reactions of the PEMFC are described as follows:

The reaction in the anode: $2H_2 \Rightarrow 4H^+ + 4e^-$.

The reaction in the cathode: $O_2 + 4H^+ + 4e^- \Rightarrow 2H_2O$.

The total reaction of the cell: $2H_2 + O_2 \Rightarrow 2H_2O$.

### 2.2.1. The PEMFC model

According to the model proposed in literature [13], the terminal voltage of the PEMFC is shown in Eq. (11). From the equation, the PEMFC is unable to generate the theoretic voltage due to three voltage losses: the activation voltage loss, the ohmic voltage loss, and the concentration voltage loss.

$$V_C = (E_{Nernst} - V_{act} - V_{ohmic} - V_{con}) \times N_S \tag{11}$$

where the $V_C$ is the terminal voltage of the cell stack, $E_{Nernst}$ is the reversible open circuit voltage, $V_{act}$ is the activation voltage loss by the anode and cathode activation, $V_{ohmic}$ is the ohmic voltage loss by the resistance of protons through the exchange membrane, $V_{con}$ is the concentration voltage loss from the transport of hydrogen and oxygen, and $N_S$ is the number of series PEM fuel cells in the stack. $E_{Nernst}$ obtained in an open circuit can be defined as a Nernst equation which is given in Eq. (12).

$$\begin{aligned} E_{Nernst} &= 1.229 - 0.85 \times 10^{-3}(T - 298.15) + 4.3085 \times 10^{-5} \\ &\quad \cdot T \cdot (\ln P_{H_2} + 0.5 \ln P_{O_2}) \end{aligned} \tag{12}$$

where $P_{O_2}$ and $P_{H_2}$ which are given by Eqs. (13) and (14) respectively, are the partial pressures of the oxygen and hydrogen, and $T$ is the temperature in Kelvin.

**Table 1**
Upper and lower ranges of the solar cell.

| Parameter | $R_S(\Omega)$ | $R_{sh}(\Omega)$ | $I_{ph}(A)$ | $I_{sd}$ (μA) | $n$ |
|---|---|---|---|---|---|
| Lower | 0 | 0 | 0 | 0 | 1 |
| Upper | 0.5 | 100 | 1 | 1 | 2 |

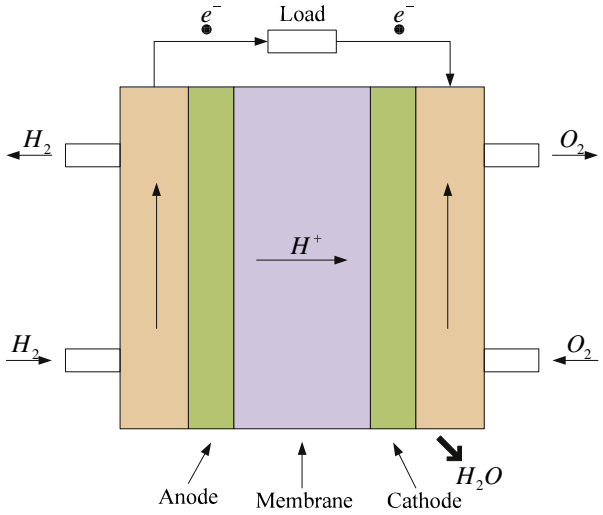


**Fig. 3.** The work process of the PEMFC.

$$P_{O_2} = (RH_c \cdot P^{sat}_{H_2O}) \cdot \left[ \frac{1}{\exp\left(\frac{4.192 \cdot (i/A)}{T^{1.334}}\right) \cdot \frac{\left(RH_c \cdot P^{sat}_{H_2O}\right)}{P_c}} - 1 \right] \quad (13)$$

$$P_{H_2} = 0.5(RH_a \cdot P^{sat}_{H_2O}) \cdot \left[ \frac{1}{\exp\left(\frac{1.635 \cdot (i/A)}{T^{1.334}}\right) \cdot \frac{\left(RH_a \cdot P^{sat}_{H_2O}\right)}{P_a}} - 1 \right] \quad (14)$$

where $P_c$ and $P_a$ are the inlet cathode and anode pressures, $RH_c$ and $RH_a$ are the relative humidity in cathode and anode, respectively, $A$ is the cell efficient active area, and $i$ is the experimental current.$P^{sat}_{H_2O}$ is the saturation pressure of water and is defined in Eq. (15).

$$\log_{10}\left(P^{sat}_{H_2O}\right) = 2.95 \times 10^{-2} \cdot (T - 273.15) - 9.18 \times 10^{-5} \cdot (T - 273.15)^2 + 1.44 \times 10^{-7} \cdot (T - 273.15)^3 - 2.18 \quad (15)$$

$V_{act}$ is the activation voltage loss which can be calculated as follows:

$$V_{act} = -\left[\xi_1 + \xi_2 \cdot T + \xi_3 \cdot T \cdot \ln\left(C_{O_2}\right) + \xi_4 \cdot T \cdot \ln(i)\right] \quad (16)$$

As shown in Eq. (16), $\xi_1, \xi_2, \xi_3$ and $\xi_4$ are the parametric coefficients based on equation with kinetic, electrochemical and thermodynamic foundations [54]. $C_{O_2}$ denotes the oxygen concentration in the catalytic interface of the cathode and is given by Eq. (17).

$$C_{O_2} = P_{O_2} / \left(5.08 \times 10^6 \exp\left(-498/T\right)\right) \quad (17)$$

In this PEMFC model, the ohmic voltage loss $V_{ohmic}$ can be defined as Eq. (18).

$$V_{ohmic} = i \cdot (R_M + R_C) \quad (18)$$

where $R_C$ is the contact resistance when the protons transfer through the membrane, and $R_M$ is the membrane resistance of the fuel cell which is given by Eq. (19).

$$R_M = \frac{\rho_M \cdot l}{A} \quad (19)$$

As shown in Eq. (19), $l$ is the thickness of the membrane. $\rho_M$ is the membrane specific resistivity and can be calculated as follows:

$$\rho_M = \frac{181.6 \cdot \left[1 + 0.03 \cdot \left(\frac{i}{A}\right) + 0.062 \cdot \left(\frac{T}{303}\right)^2 \left(\frac{i}{A}\right)^{2.5}\right]}{\left[\lambda - 0.634 - 3 \cdot \left(\frac{i}{A}\right)\right] \cdot \exp\left[4.18 \cdot \left(\frac{T-303}{T}\right)\right]} \quad (20)$$

where $\lambda$ is the adjustable parameter influenced by the preparation of the anode gas. The concentration voltage loss $V_{con}$ is shown in Eq. (21):

$$V_{con} = -b \ln\left(1 - \frac{i/A}{I_{\max}}\right) \quad (21)$$

where $b$ is the concentration loss constant and $I_{\max}$ is the maximum current density.

#### 2.2.2. The objective function

The objective function for PEMFC problem is to minimize the error between the simulated terminal voltage and the actual data obtained from the $V$–$I$ characteristics of the fuel cell [22]. To fit the actual data, it is necessary to optimize the seven parameters ($\xi_1, \xi_2, \xi_3, \xi_4, \lambda, R_C, b$) from Eqs. (11)–(21). The objective function is given as follows:

$$F_{fc} = \min_{(\xi_1,\xi_2,\xi_3,\xi_4,\lambda,R_C,b)} \left( \sum_{i=1}^{N} \sum_{j=1}^{M} (V_{actual} - V_C)^2 \right) \quad (22)$$

where $V_C$ is the voltage calculated by Eq. (11), $V_{actual}$ is the experimental voltage, $N$ is the number of the experimental data groups used in optimization and $M$ is the number of the experimental data points in each group. In this research, two possible ranges for these parameters are provided from the literatures [22,23] as in Table 2. Other model parameters and operating conditions are described in Table 3.

## 3. Methodology

### 3.1. Biogeography-based optimization

Biogeography-based optimization (BBO) is based on the theory of island biogeography which uses mathematical models of biogeography to describe how species migrate from one island to another, how new species arise, and how species become extinct [39]. In BBO, each individual is regarded as an island with a habitat suitability index (HSI) and each variable of an island is called suitability index variable (SIV). A good solution means that the island with a high HSI has a large number of species, while a poor solution indicates the island with a low HSI has a small number of species. Therefore, species in the high HSI islands often migrate to low HSI islands and the low HSI islands accepts immigrants from high HSI islands.

#### 3.1.1. Migration

In biogeography-based optimization, each island has its own immigration rate $\lambda$ and emigration $\mu$ which are the functions of species in the habitat. Fig. 4 illustrates the relationship between

**Table 2**
Tow parameter ranges of the PEMFC.

| Parameter | $\xi_1$ | $\xi_1$ | $\xi_1$ | $\xi_1$ | $\lambda$ | $R_C$ | $b$ |
|---|---|---|---|---|---|---|---|
| Range1, min | −1.19969 | 0.001 | 3.60e−5 | −2.60e−4 | 10 | 0.0001 | 0.0136 |
| Range1, max | −0.8532 | 0.005 | 9.80e−5 | −9.54e−5 | 24 | 0.0008 | 0.5 |
| Range2, min | −0.952 | 0.001 | 7.40e−5 | −1.98e−4 | 14 | 0.0001 | 0.016 |
| Range2, max | −0.944 | 0.005 | 7.80e−5 | −1.88e−4 | 23 | 0.0008 | 0.5 |

**Table 3**
Other parameters and operating conditions.

| Parameter | Value | Parameter | Conditions |
|---|---|---|---|
| $N_S$ | 24 | $P_a$ (*bar*) | 1.0–3.0 |
| $A$ (cm$^2$) | 27 | $P_c$ (*bar*) | 1.0–5.0 |
| $l$ (μm) | 127 | T (*K*) | 343.15–353.15 |
| $I_{max}$ (A/cm$^2$) | 0.860 | $RH_a$ | 1 |
| Rater power (*W*) | 250 | $RH_c$ | 1 |

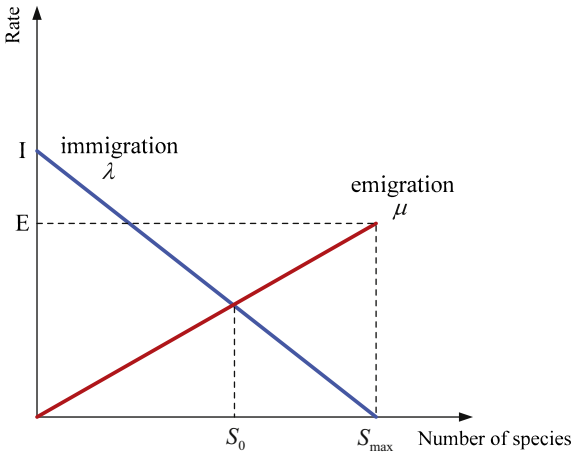


**Fig. 4.** Relationship between species count.

species count, immigration rate and emigration rate. The functions of immigration rate and emigration rate can be defined as:

$$\lambda_s = I\left(1 - \frac{s}{n}\right) \tag{23}$$

$$\mu_s = E\left(\frac{s}{n}\right) \tag{24}$$

where $I$ denotes the maximum possible immigration rate which occurs when there are no species in the island, $E$ is the maximum emigration rate which occurs when the island has the largest number of species, $s$ is the number of species of the $s$th individual in the ordered population according to the fitness, and $n$ is the number of candidate solutions in the population. $I$ and $E$ are usually set equal to 1. The immigration and emigration rates of each solution are used to share information between islands. The immigration rate $\lambda$ decides whether or not to modify each suitability index variable (SIV) in the selected solution. The emigration rate $\mu$ decides which of the solutions should migrate a random SIV to the selected solution.

### 3.1.2. Mutation

In nature, cataclysmic events can drastically change the solution of an island. An island's HSI can, therefore, change suddenly as a result of random events. So mutation is introduced to BBO algorithm and mutation rates are determined by species count probabilities. The species count probability $P_s$ means the island contains $S$ species probability and its change rate can be calculated as:

$$\dot{P}_s = \begin{cases} -(\lambda_s + \mu_s)P_s + \mu_{s+1}P_{s+1}, & S = 0 \\ -(\lambda_s + \mu_s)P_s + \lambda_{s+1}P_{s-1} + \mu_{s+1}P_{s+1}, & 1 \leqslant S \leqslant S_{max} - 1 \\ -(\lambda_s + \mu_s)P_s + \lambda_{s+1}P_{s-1}, & S = S_{max} \end{cases} \tag{25}$$

where $\lambda_s$ and $\mu_s$ are the immigration and emigration rates when there are $S$ species in the island, and $S_{max}$ denotes the maximal species in the island.

Hybrid migration of BBO-M

**For** each island (solution)
  Select randomly $r_1$ th island;
  **For** each SIV (solution variable)
    Select $H_i$ with probability $\propto \lambda_i$;
    **If** $H_i$ is selected **then**
      Select $H_j$ with probability $\propto \mu_i$;
      **If** $H_j$ is selected **then**
        Generate number *rand* randomly between 0 and 1;
        $H_{newi} = H_i + rand \times (H_j - H_{r1})$;
      **End if**
    **End if**
  **End for**
**End for**

**Fig. 5.** Hybrid migration of BBO-M.

Each solution has a mutation rate based on its own species count probability. If the probability $P_s$ in a solution $S$ low, it is likely to mutate to some other solutions. On the contrary, high probability is less likely to mutate the solution to a different one. The mutation rates can be proportional to the species count probabilities as:

$$m(S) = m_{max}\left(\frac{1 - P_s}{P_{max}}\right) \tag{26}$$

where $m_{max}$ is the maximal mutation rate defined by user, and $P_{max}$ is the maximal species count probability. This mutation operator increases diversity of the population. It makes low HSI islands have a chance to improve and gives high HSI islands a chance to progress better than they already have.

### 3.2. Proposed BBO with mutation strategies method

In conventional BBO, there are two main operators, the migration and the mutation. In terms of BBO migration, solutions can share their information with each other. Especially, good solutions tend to migrate useful information to poor solutions [39]. This makes BBO good at exploring the solutions of the current population. Although BBO has been applied to real world problems, and has demonstrated the potential in finding the optimal solutions rapidly, it has some main disadvantages [46]:

1. BBO is poor in exploiting the solutions;
2. The best members are not selected from each generation;
3. A solution does not consider its fitness, as a result many infeasible solutions are generated.

To overcome these defects, some strategies are introduced into the migration and mutation phases in BBO in this paper. BBO with mutation strategies (BBO-M) proposed here integrates the exploration of the BBO and the exploitation of mutation strategies. The approach of BBO-M is described as follows.

### 3.2.1. Hybrid migration

The main operator of the BBO is the migration operator, which uses emigration to select relatively better solutions to replace the solutions selected by immigration. This operator only exchanges the information between the good solutions and poor solutions, but does not generate new HSI, so it is easy to produce the premature convergence. To solve it, original migration is replaced by a hybrid migration which is motivated by mutation in DE algorithm. In the mutation of DE, the offsprings are determined by three parents' genes. With this ideal, the hybrid migration of BBO-M

Hybrid mutation of BBO-M

Randomly generate a initial value $x_0 \neq 0, 0.25, 0.5, 0.75, 1$;
**For** each island (solution)
  **For** each SIV (solution variable)
    Select $H_i(SIV)$ based on mutation probability $m_i$;
    **If** $H_i(SIV)$ is selected **then**
      $H_{newi}(SIV) = H_i(SIV) + (1 - 2x)$
    **End if**
  **End for**
**End for**
Update the $x$ using logistic equation

**Fig. 6.** Hybrid mutation of BBO-M.

dose not simply replace the solution $H_j$ to the solution $H_i$. Instead, a new solution HSI of BBO-M is comprised three parts: a solution selected by emigration, a solution selected randomly and itself. The hybrid migration is defined in Fig. 5.

The hybrid migration operator is based on two considerations. Firstly, a new offspring not only contains the features of poor solution, but also accepts some information from the good solution. Secondly, the hybrid migration of BBO-M is capable of balancing the exploitation and exploration capabilities, thus makes the algorithm more robust.

### 3.2.2. Hybrid mutation

The mutation in original BBO is that the features selected by mutation probability are replaced with randomly generated ones. Although this operator can generate different solutions, the current good solutions may be destroyed by the randomly generated operations. To reduce the possibilities of these effects, the conventional mutation is replaced by a new solution using chaos theory. Assume that the current optimal solution is closed to the final best after a certain number of loops, then a good chaotic disturbance variable is added to the current optimal solution to find the final optimal solution. The mutation with chaos theory is a mild regulation which is not the same as the random mutation. It improves the exploration of BBO-M, and affects barely the current good solution.

BBO-M algorithm

Create a random set of islands (population) $H_1, H_2, ..., H_n$;
Compute HSI values;
Randomly generate a initial value $x_0 \neq 0, 0.25, 0.5, 0.75, 1$;
**While** the halting criterion is not satisfied **do**
  Sort the population from best to worst
  For each island , map the HSI to the number of species
  Compute immigration rate $\lambda$ and emigration rate $\mu$ for each island based on HSI;
  Modify the population with the hybrid migration operator shown in Fig 5;
  Modify the population with the hybrid mutation operator shown in Fig 6;
  Compute HSI values;
  Boundary constraints:

$$\begin{cases} H_{newi} = U_{\max} & if\ H_{newi} > U_{\max} \\ H_{newi} = U_{\min} & if\ H_{newi} < U_{\min} \end{cases}$$

  ($U_{\min}$ and $U_{\max}$ are the upper and lower bounds of the searching space.)
  **For** each island (solution)
    **If** the new $H_{newi}$ is better than $H_i$ **then**
      $H_i = H_{newi}$;
    **End if**
  **End for**
**End while**

**Fig. 7.** BBO-M algorithm.

**Table 4**
Formulations of Benchmark functions.

| No. | Function | Formulation | Type | Dim | Boundary | $f_{\min}$ |
|---|---|---|---|---|---|---|
| 1 | Sphere | $f_1(\mathbf{x}) = \sum_{i=1}^{Dim} x_i^2$ | Unimodal | 50 | $[-100, 100]$ | 0 |
| 2 | Schwefel 2.22 | $f_2 = \sum_{i=1}^{D} \lvert x_i \rvert + \prod_{i=1}^{D} \lvert x_i \rvert$ | Unimodal | 50 | $[-100, 100]$ | 0 |
| 3 | Schwefel 2.21 | $f_3(\mathbf{x}) = max\{\lvert x_i \rvert, 1 \leqslant i \leqslant Dim\}$ | Unimodal | 50 | $[-100, 100]$ | 0 |
| 4 | Axis | $f_4 = \sum_{i=1}^{D} i x_i^2$ | Unimodal | 50 | $[-100, 100]$ | 0 |
| 5 | Quatic | $f_5(\mathbf{x}) = \sum_{i=1}^{Dim} i x_i^4$ | Unimodal | 50 | $[-1.28, 1.28]$ | 0 |
| 6 | Rosenbrock | $f_6(\mathbf{x}) = \sum_{i=1}^{Dim-1} \left\{ 100 \cdot (x_{i+1} - y_i)^2 + (1 - x_i)^2 \right\}$ | Multimodal | 50 | $[-30, 30]$ | 0 |
| 7 | Rastrigin | $f_7(\mathbf{x}) = \sum_{i=1}^{Dim} \{x_i^2 - 10\cos(2\pi x_i) + 10\}$ | Multimodal | 50 | $[-5.12, 5.12]$ | 0 |
| 8 | Griewank | $f_8(\mathbf{x}) = \sum_{i=1}^{Dim} \frac{x_i^2}{4000} - \prod_{i=1}^{Dim} \cos\left(\frac{x_i}{\sqrt{i}}\right) + 1$ | Multimodal | 50 | $[-600, 600]$ | 0 |
| 9 | Ackley | $f_9(\mathbf{x}) = -20\exp\left(-0.2\sqrt{\frac{1}{Dim}\sum_{i=1}^{Dim} x_i^2}\right) - \exp\left(\frac{1}{Dim}\sum_{i=1}^{Dim}\cos(2\pi x_i)\right) + 20 + e$ | Multimodal | 50 | $[-32, 32]$ | 0 |
| 10 | Step | $f_{10}(\mathbf{x}) = \sum_{i=1}^{Dim} x_i (\lfloor x_i + 0.5 \rfloor)^2$ | Discontinuous | 50 | $[-100, 100]$ | 0 |

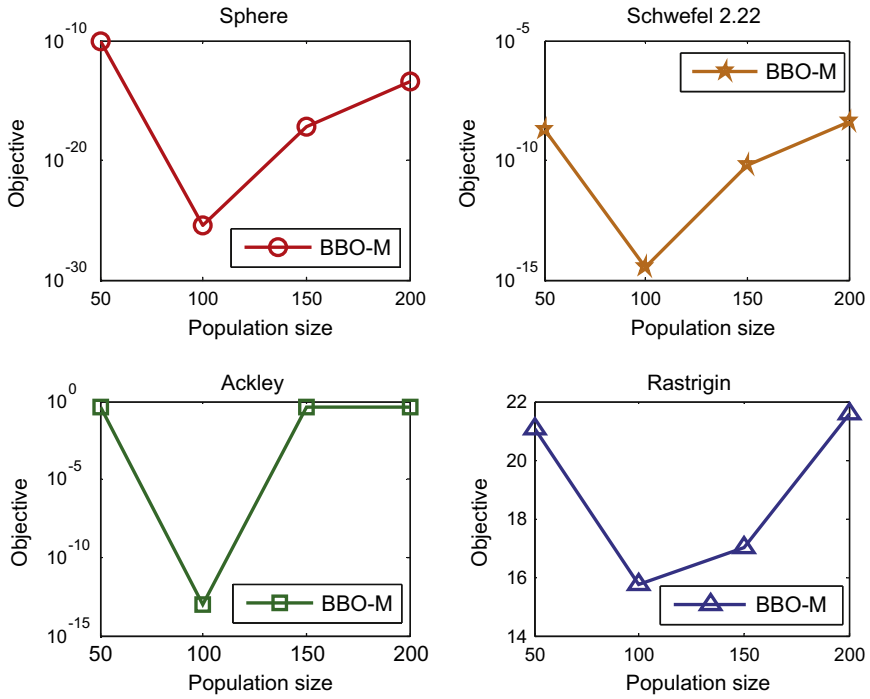


**Fig. 8.** Mean results obtained by BBO-M on four test problems with different *N*.

There are a number of mapping methods in the chaos theory up till now. In the paper, the well-known logistic equation [47], which is one of the mapping methods in the chaos theory, is employed. The logistic equation is defined in Eq. (27).

$$x_{n+1} = \mu \cdot x_n(1 - x_n), \quad 0 \leqslant x_0 \leqslant 1 \tag{27}$$

where $\mu$ is the control parameter which is often equal to 4 for full range of mapping, and $x$ is a variable between 0 and 1. From the logistic equation, the initial value does not include the five fixed points (0, 0.25, 0.5, 0.75, 1). The hybrid mutation is described in Fig. 6.

From the analysis of BBO-M, it can be seen that the BBO with mutation strategies not only keeps the advantages of conventional BBO, but also integrates other advantages from mutation strategies. The whole BBO-M algorithm is defined as Fig. 7.

## 4. Numerical experiments and results

In this section, ten commonly used benchmark functions chosen from [40,41] in Table 4 are used to test the performance of the proposed BBO-M. According to their properties, these functions are divided into three groups: $f_1 - f_5$ are unimodal problems, $f_6 - f_9$ are multimodal problems, and $f_{10}$ is a unimodal and discontinuous problem. All functions are tested on 50 dimensions (50 variables) by 50 independent runs. For each run, the maximum number of fitness evaluations, the Max FES is set to 300,000.

### 4.1. Parameter setting

The parameters of BBO-M are the same as BBO in literature [39] except for the population size *N*. In order to investigate an appropriate *Ns* for BBO-M, $f_1, f_2, f_7$ and $f_9$ are used to test the objective values with *N* 50, 100, 150, 200 respectively. Fig. 8 illustrates the mean values of the 50 runs of the BBO-M on four test functions with 50 dimensions. It is obvious that the population size has significant impact on the performance of BBO-M. When the *N* is set to 100, the BBO-M achieves the best mean results on all these test problems. Hence, the population size *N* is set to 100 for the BBO-M in this paper.

**Table 5**
Control parameters.

| Algorithm | Parameters |
|---|---|
| BBO [39] | Habitat modification probability = 1;<br>Immigration probability bound per gene = [0,1];<br>Step size for numerical integration of probability = 1;<br>Mutation probability $m_{\max} = 0.005$;<br>Maximal immigration rate $I = 1$;<br>Maximal emigration rate $E = 1$;<br>Elitism parameter keep = 2;<br>Population size $N = 50$; |
| BBO-M | The same with BBO only population size $N = 100$. |
| DE [48] | Mutation factor $F = 0.5$;<br>Crossover constant $CR = 0.3$;<br>Population size $N = 100$. |
| GHS [49] | Considering rate of harmony memory $HMCR = 0.9$;<br>Bounds of pitch adjustment rate $PAR_{max} = 0.99$ and $PAR_{min} = 0.01$;<br>Population size $N = 5$. |
| PSO-w [50] | Learning factors $C_1 = C_2 = 2$;<br>Inertia weight $w$ taken from 0.9 to 0.4;<br>Population size $N = 30$. |
| GA toolbox [51] | Crossover probability $P_c = 0.7$;<br>Mutation probability $P_m = P_c$/Dimension = 0.014;<br>Population size $N = 50$. |

### 4.2. Benchmark experiments

In the numerical experiments, the BBO-M is compared with BBO [39], DE [48], GHS [49], PSO-w [50] and GA toolbox [51]. The control parameters in these algorithms are given in Table 5, which are in accordance with the references. All the experiments are carried out using Matlab 7.7.0 (R2008b) and programs are executed on an Pentium (R) Dual-Core 2.60 GHz CPU and 2.00 GB RAM personal computer.

Table 6 presents the means and standard deviation of the 50 runs of the six algorithms on the ten functions with 50 dimensions. The best results among the six algorithms are shown in bold. In order to illustrate the convergence characteristics, the medians of each algorithm for four test functions from the three different types are chosen ((a) Sphere function, (b) Rosenbrock function, (c) Ackley function, (d) Step function.). From the results, it can be observed that for the unimodal problems, BBO-M achieves better performance on most functions $f_1, f_2, f_4, f_5$ and the improvement is most significant on functions $f_1$ and $f_5$. On multimodal groups, BBO-M also outperforms the conventional BBO and GA. For example, BBO-M the optimum value for function $f_9$ is 8.61e−14 which has great improvement than other algorithms. The BBO-M achieves the same best result as the DE and GHS on unimodal and discontinuous function $f_{10}$, and they are all much better than other algorithms on this function. DE and HGS also perform well on functions $f_3, f_7$ and $f_8$ respectively. However, the BBO-M performs better on more complex problems while the other algorithms can be trapped into local optimum.

## 5. Parameter identifications and results

For parameter identifications, the control parameters for BBO-M, BBO, DE, PSO-w and GHS are the same with those in Section 4. The Max FES is set to 80,000 for solar cell models and 8000 for PEMFC model. Matlab 7.7.0 (R2008b) is also used for parameter identifications in the same personal computer.

### 5.1. Solar cell models

The *V–I* characteristic of a silicon solar cell is used to evaluate the efficiency of the proposed BBO-M parameter estimation method. The experimental data is taken from [14]. Table 7 summarizes the optimal parameters and the value $F_{min}$ of the double diode model obtained by BBO-M compared with BBO and DE. The results are also compared with ABSO [38], PS [37], SA [24] and HS [38]. It is obvious that BBO-M outperforms BBO, DE, ABSO, PS, SA and HS as it has found the minimum value $F_{min}$. Table 8 shows the results of the single diode model obtained by BBO-M in comparison with

**Table 6**
Experiment result of 6 different methods over 50 runs on ten 50-D functions.

| Function | | BBO-M | BBO | DE | GHS | PSO-w | GA |
|---|---|---|---|---|---|---|---|
| $f_1$ | Mean | **3.38e−26** | 3.9439 | 1.37e−24 | 2.53e−2 | 5.18e−19 | 4.54e−7 |
| | Std | 1.16e−25 | 1.2672 | 6.71e−25 | 6.21e−2 | 1.39e−18 | 4.54e−7 |
| $f_2$ | Mean | **3.14e−15** | 1.0079 | 8.85e−15 | 6.12e−2 | 1.42e−13 | 4.76e−4 |
| | Std | 1.09e−15 | 1.31e−1 | 1.87e−15 | 7.05e−2 | 2.48e−13 | 0.0000 |
| $f_3$ | Mean | 2.56e+1 | 8.4974 | **2.91e−1** | 1.25e+1 | 5.4059 | 4.1017 |
| | Std | 8.3555 | 1.1939 | 3.59e−2 | 5.5576 | 6.71e−1 | 1.2125 |
| $f_4$ | Mean | **5.80e−26** | 2.66e−1 | 7.28e−26 | 1.03e−3 | 2.90e−20 | 3.03e−8 |
| | Std | 3.39e−25 | 8.44e−2 | 3.16e−26 | 1.46e−3 | 6.13e−20 | 0.0000 |
| $f_5$ | Mean | **1.19e−46** | 1.20e−6 | 9.98e−40 | 1.42e−10 | 9.26e−26 | 2.83e−21 |
| | Std | 7.33e−46 | 1.25e−6 | 8.42e−40 | 5.70e−10 | 5.19e−25 | 3.79e−37 |
| $f_6$ | Mean | **4.01e+1** | 3.61e+2 | 4.32e+1 | 1.42e+2 | 8.23e+1 | 6.11e+1 |
| | Std | 3.29e+1 | 9.78e+1 | 4.60e−1 | 1.65e+2 | 3.70e+1 | 4.34e+1 |
| $f_7$ | Mean | 1.57e+1 | 3.8575 | 1.83e+2 | **1.40e−2** | 8.03e+1 | 8.45e+1 |
| | Std | 9.2553 | 6.55e−1 | 8.7867 | 4.19e−2 | 1.77e+1 | 1.37e+1 |
| $f_8$ | Mean | 7.90e−3 | 1.0702 | **0.0000** | 8.30e−2 | 8.56e−3 | 3.97e−2 |
| | Std | 1.13e−2 | 3.07e−2 | 0.0000 | 1.44e−1 | 1.19e−2 | 3.96e−2 |
| $f_9$ | Mean | **8.61e−14** | 6.70e−1 | 2.43e−13 | 1.94e−2 | 8.42e−11 | 1.22e−4 |
| | Std | 1.58e−14 | 1.14e−1 | 4.51e−14 | 1.96e−2 | 7.46e−11 | 0.0000 |
| $f_{10}$ | Mean | **0.0000** | 4.2000 | **0.0000** | **0.0000** | 2.00e−2 | 7.75e+1 |
| | Std | 0.0000 | 1.7379 | 0.0000 | 0.0000 | 1.41e−1 | 3.62e+2 |

The bold values can show the best results of the correspongding benchmark function clearly.

**Table 7**
Results of parameter identification for double diode model.

| Item | BBO-M | BBO | DE | ABSO [38] | PS [37] | SA [24] | HS [38] |
|---|---|---|---|---|---|---|---|
| $R_S(\Omega)$ | 0.03664 | 0.03673 | 0.03661 | 0.03657 | 0.0320 | 0.0345 | 0.03545 |
| $R_{sh}(\Omega)$ | 55.0494 | 58.4585 | 56.0213 | 54.6219 | 81.3008 | 43.1034 | 46.8269 |
| $I_{ph}(A)$ | 0.76083 | 0.75940 | 0.76079 | 0.76078 | 0.7602 | 0.7623 | 0.76176 |
| $I_{sd1}$ (μA) | 0.59115 | 0.95830 | 0.36605 | 0.26713 | 0.9889 | 0.4767 | 0.12545 |
| $I_{sd2}$ (μA) | 0.24523 | 0.14885 | 0.26320 | 0.38191 | 0.0001 | 0.0100 | 0.25470 |
| $n_1$ | 2.00000 | 1.85714 | 1.91164 | 1.46512 | 1.6000 | 1.5172 | 1.49439 |
| $n_2$ | 1.45798 | 1.42309 | 1.46500 | 1.98152 | 1.1920 | 2.0000 | 1.49989 |
| $F_{\min}$ | 9.8272e-4 | 0.0016 | 0.0010 | 9.8344e-4 | 0.01518 | 0.01664 | 0.00126 |

**Table 8**
Results of parameter identification for single diode model.

| Item | BBO-M | BBO | DE | IADE [31] | ABSO [38] | CPSO [26] | GA [20] | PS [37] | SA [24] | HS [38] |
|---|---|---|---|---|---|---|---|---|---|---|
| $R_S(\Omega)$ | 0.03642 | 0.03214 | 0.03598 | 0.03621 | 0.03659 | 0.0354 | 0.0299 | 0.0313 | 0.0345 | 0.03663 |
| $R_{sh}(\Omega)$ | 53.36227 | 78.8555 | 56.5533 | 54.7643 | 52.2903 | 59.012 | 42.3729 | 64.1026 | 43.1034 | 53.5946 |
| $I_{ph}$ (A) | 0.76078 | 0.76098 | 0.76068 | 0.7607 | 0.76080 | 0.7607 | 0.7619 | 0.7617 | 0.7620 | 0.76070 |
| $I_{sd}$ (μA) | 0.31874 | 0.86100 | 0.35515 | 0.33613 | 0.30623 | 0.4000 | 0.8087 | 0.9980 | 0.4798 | 0.30495 |
| $n$ | 1.47984 | 1.58742 | 1.49080 | 1.4852 | 1.47583 | 1.5033 | 1.5751 | 1.6000 | 1.5172 | 1.47538 |
| $F_{\min}$ | 9.8634e−4 | 0.00238 | 0.00100 | 9.8900e−4 | 9.9124e−4 | 0.00139 | 0.01908 | 0.01494 | 0.01900 | 9.9510e−4 |

BBO, DE, ABSO [38], PS [37], SA [24] and HS [38]. It is also compared with chaos particle swarm optimization algorithm (CPSO) [26], improved adaptive differential evolution (IADE) [31], and genetic algorithm [20]. The BBO-M yields better results than BBO, DE, IADE, ABSO, CPSO, GA, PS, SA and HS. As a result, the optimal parameters found by BBO-M are closer to the experimental parameters of the system.

In order to further confirm the quality of the identification results, the parameters obtained by BBO-M are used to calculate the currents $I_t$ shown in Tables 9 and 10. The relative error, $I_{t-measured} - I_{t-calculated}$, demonstrates the high accuracy of the identified model. The identified parameters are also employed to reconstruct the $I$–$V$ characteristic as shown in Figs. 9a and 10a. It can be seen that the resultant model is in good agreement with the experimental data. The power vs. voltage ($P$–$V$) characteristic of the system is also shown in Figs. 9b and 10b. The similarity between the calculated results and the measured data of the real system proves the superiority of the identification results using the proposed method. Fig. 11 illustrate the evolving processes of three methods with experimental $I$–$V$ data for both the single and the double diode models. Obviously, in this case, the BBO-M algorithm also converges more rapidly than BBO and DE (see Fig. 11).

**Table 9**
Relative error for double diode model.

| Measurement | $V_t$ ($V$) | $I_t$ measured (A) | $I_t$ calculated (A) | Relative error |
|---|---|---|---|---|
| 1 | −0.2057 | 0.7640 | 0.764012 | −0.000012 |
| 2 | −0.1291 | 0.7620 | 0.762622 | −0.000622 |
| 3 | −0.0588 | 0.7605 | 0.761345 | −0.000845 |
| 4 | 0.0057 | 0.7605 | 0.760172 | 0.000327 |
| 5 | 0.0646 | 0.7600 | 0.759098 | 0.000901 |
| 6 | 0.1185 | 0.7590 | 0.758106 | 0.000893 |
| 7 | 0.1678 | 0.7570 | 0.757168 | −0.000168 |
| 8 | 0.2132 | 0.7570 | 0.756221 | 0.000778 |
| 9 | 0.2545 | 0.7555 | 0.755157 | 0.000342 |
| 10 | 0.2924 | 0.7540 | 0.753708 | 0.000291 |
| 11 | 0.3269 | 0.7505 | 0.751395 | −0.000895 |
| 12 | 0.3585 | 0.7465 | 0.747310 | −0.000810 |
| 13 | 0.3873 | 0.7385 | 0.740029 | −0.001529 |
| 14 | 0.4137 | 0.7280 | 0.727270 | 0.000729 |
| 15 | 0.4373 | 0.7065 | 0.706869 | −0.000369 |
| 16 | 0.4590 | 0.6755 | 0.675217 | 0.000282 |
| 17 | 0.4784 | 0.6320 | 0.630753 | 0.001246 |
| 18 | 0.4960 | 0.5730 | 0.571976 | 0.001023 |
| 19 | 0.5119 | 0.4990 | 0.499685 | −0.000685 |
| 20 | 0.5265 | 0.4130 | 0.413723 | −0.000723 |
| 21 | 0.5398 | 0.3165 | 0.317553 | −0.001053 |
| 22 | 0.5521 | 0.2120 | 0.212151 | −0.000151 |
| 23 | 0.5633 | 0.1335 | 0.102208 | 0.001291 |
| 24 | 0.5736 | −0.0100 | −0.008750 | −0.001249 |
| 25 | 0.5833 | −0.1230 | −0.125513 | 0.002513 |
| 26 | 0.5900 | −0.2100 | −0.208379 | −0.001620 |

**Table 10**
Relative error for single diode model.

| Measurement | $V_t$ ($V$) | $I_t$ measured (A) | $I_t$ calculated (A) | Relative error |
|---|---|---|---|---|
| 1 | −0.2057 | 0.7640 | 0.764006 | −0.000006 |
| 2 | −0.1291 | 0.7620 | 0.762604 | −0.000604 |
| 3 | −0.0588 | 0.7605 | 0.761317 | −0.000817 |
| 4 | 0.0057 | 0.7605 | 0.760135 | 0.000364 |
| 5 | 0.0646 | 0.7600 | 0.759053 | 0.000946 |
| 6 | 0.1185 | 0.7590 | 0.758056 | 0.000943 |
| 7 | 0.1678 | 0.7570 | 0.757120 | −0.000120 |
| 8 | 0.2132 | 0.7570 | 0.756182 | 0.000817 |
| 9 | 0.2545 | 0.7555 | 0.755138 | 0.000361 |
| 10 | 0.2924 | 0.7540 | 0.753723 | 0.000276 |
| 11 | 0.3269 | 0.7505 | 0.751453 | −0.000953 |
| 12 | 0.3585 | 0.7465 | 0.747414 | −0.000914 |
| 13 | 0.3873 | 0.7385 | 0.740168 | −0.001668 |
| 14 | 0.4137 | 0.7280 | 0.727416 | 0.000583 |
| 15 | 0.4373 | 0.7065 | 0.706985 | −0.000485 |
| 16 | 0.4590 | 0.6755 | 0.675269 | 0.000230 |
| 17 | 0.4784 | 0.6320 | 0.630728 | 0.001271 |
| 18 | 0.4960 | 0.5730 | 0.571887 | 0.001112 |
| 19 | 0.5119 | 0.4990 | 0.499563 | −0.000563 |
| 20 | 0.5265 | 0.4130 | 0.413612 | −0.000612 |
| 21 | 0.5398 | 0.3165 | 0.317485 | −0.000985 |
| 22 | 0.5521 | 0.2120 | 0.212142 | −0.000142 |
| 23 | 0.5633 | 0.1335 | 0.102245 | 0.001254 |
| 24 | 0.5736 | −0.0100 | −0.008731 | −0.001268 |
| 25 | 0.5833 | −0.1230 | −0.125537 | 0.002537 |
| 26 | 0.5900 | −0.2100 | −0.208530 | −0.001469 |

### 5.2. PEM fuel cell model

In this section, Eqs. (11)–(22) are used to solve the parameter identification problem for the PEMFC stack model. In this study, two possible ranges of parameters taken from the literatures are given in Table 2. For these operational ranges, four sets of *V–I* experimental data, which are taken from [23], are used for parameter optimization. Two sets of data (3/5 bar 353.15 K, 1/1 bar 343.15 K) are used to determine the optimal parameters, and other two sets of data (2.5/3 bar 343.15 K, 1.5/1.5 bar 343.15 K) are used for model validation. It should be noticed that these four data originates from the graphical diagrams, and some extra variability may be caused by this procedure [21,23].

Under the range 1 from Table 2, seven parameters ($\xi_1, \xi_2, \xi_3, \xi_4, \lambda, R_C, b$) of the model are optimized by BBO-M, conventional BBO, DE, PSO-w and GHS, and are compared with the results of real-coded genetic algorithm (RGA) [23]. All the produced parameters are presented in Table 11, and the value $F_{min}$ is the sum of the squared error for all four data sets between the PEMFC model output voltages and the experimental PEMFC output voltages. It is obvious that the value 7.6165 by BBO-M is the best, which is less than that results obtained by BBO (8.0518), DE (8.3656), PSO-w (8.2893) and GHS (8.2954), and than the results by RGA which are 8.4854. From Table 11, it is obvious that BBO-M performs the best.

The range 2 in Table 2 is also used for PEMFC model parameter estimation. In this range, the optimized parameters obtained by BBO-M are compared with that found by the conventional BBO, DE, PSO-w, GHS and RGA [23]. The performance of these algorithms on the parameters identification of PEMFC model is shown in Table 12. Based on the results, it is clear that BBO-M is superior to BBO and other reported algorithms.

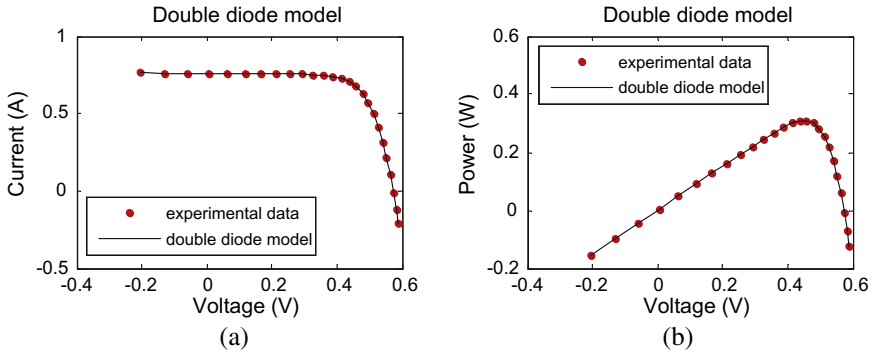


**Fig. 9.** (a) The double diode model *I–V* curve and experimental data. (b) The double diode model *P–V* curve and experimental data.

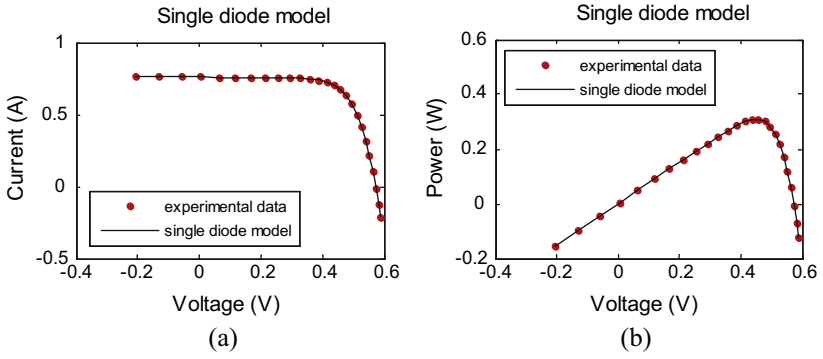


**Fig. 10.** (a) The single diode model *I–V* curve and experimental data. (b) The single diode model *P–V* curve and experimental data.

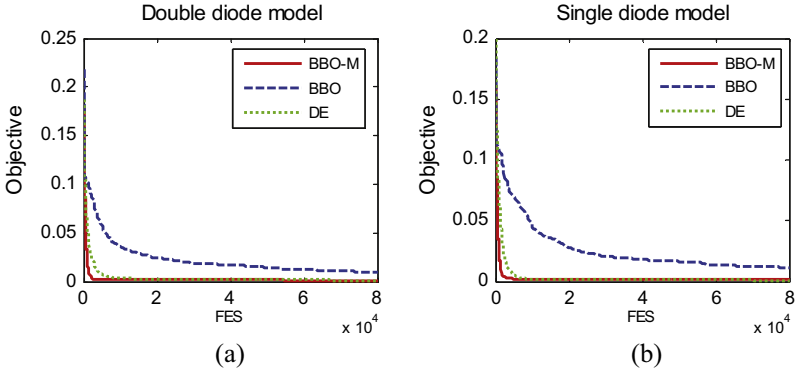


**Fig. 11.** (a) Convergence graphs of double diode solar cell. (b) Convergence graphs of single diode solar cell.

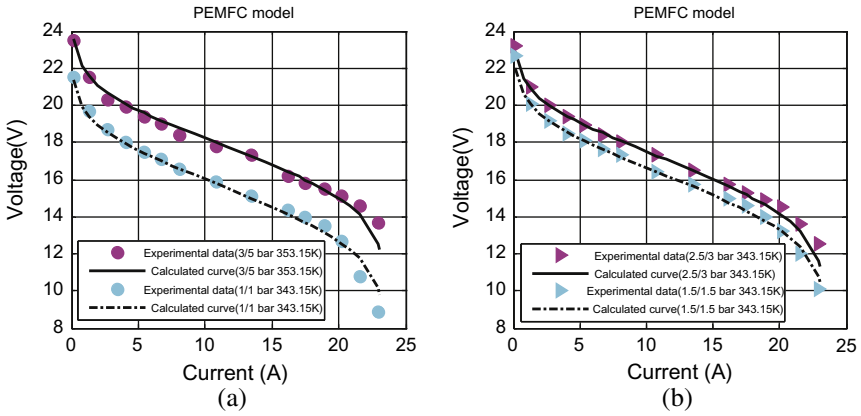


**Fig. 12.** (a) PEMFC *I–V* curve and experimental data (Identification). (b) PEMFC *P–V* curve and experimental data (Validation).

The correct parameter range for the search is essential in these algorithms. Firstly, the range should be wide enough to cover the true values of the parameters. Secondly, when parameters with some physical meaning are in questions, their values should at least be feasible. In this study, the best value of $F_{min}$ for range 1 is 7.6165 and the best value of $F_{min}$ for range 2 is 16.2363. From Tables 11 and 12, it can be seen that range 1 leads to considerable smaller values of the objective function in all cases. In order to make a comparison between the calculated voltages and the experimental voltages, the parameters optimized by BBO-M with range 1 are used to describe the *I–V* characteristic curves of four sets data in Fig. 12, and these model parameters give a good reflection of the

**Table 11**
Results of parameter identification for PEMFC with range 1.

| Item | $\xi_1$ | $\xi_2$ | $\xi_3$ | $\xi_4$ | $\lambda$ | $R_C$ | $b$ | $F_{\min}$ |
|---|---|---|---|---|---|---|---|---|
| BBO-M | −0.8574 | 2.5910e−3 | 7.6514e−5 | −1.1580e−4 | 12.7455 | 1.0029e−4 | 3.3368e−2 | 7.6165 |
| BBO | −0.8566 | 2.4981e−3 | 6.8156e−5 | −1.1851e−4 | 12.5678 | 3.0080e−4 | 3.3307e−2 | 8.0518 |
| DE | −1.1355 | 3.2336e−3 | 6.5181e−5 | −1.1604e−4 | 14.9740 | 3.6894e−4 | 3.7305e−2 | 8.3656 |
| PSO-w | −1.0446 | 3.0047e−3 | 6.7196e−5 | −1.1544e−4 | 12.4944 | 1.0000e−4 | 3.2563e−2 | 8.2893 |
| GHS | −1.0072 | 2.9755e−3 | 7.1777e−5 | −1.2612e−4 | 15.5959 | 8.0000e−4 | 3.7341e−2 | 8.2954 |
| RGA [23] | −1.1568 | 3.4243e−3 | 6.4161e−5 | −1.1544e−4 | 12.8989 | 1.4504e−4 | 3.4300e−2 | 8.4854 |

**Table 12**
Results of parameter identification for PEMFC with range 2.

| Item | $\xi_1$ | $\xi_2$ | $\xi_3$ | $\xi_4$ | $\lambda$ | $R_C$ | $b$ | $F_{\min}$ |
|---|---|---|---|---|---|---|---|---|
| BBO-M | −0.9520 | 2.9400e−3 | 7.8000e−5 | −1.8800e−4 | 23.0000 | 1.0000e−4 | 3.2813e−2 | 16.2363 |
| BBO | −0.9459 | 2.9207e−3 | 7.7366e−5 | −1.8827e−4 | 22.6510 | 1.4110e−4 | 3.3410e−2 | 16.4955 |
| DE | −0.9520 | 2.9399e−3 | 7.8000e−5 | −1.8800e−4 | 23.0000 | 1.0000e−4 | 3.2839e−2 | 16.2425 |
| PSO-w | −0.9473 | 2.9263e−3 | 7.7987e−5 | −1.8800e−4 | 22.9508 | 1.3142e−4 | 3.2528e−2 | 16.3446 |
| GHS | −0.9513 | 2.9359e−3 | 7.8000e−5 | −1.8800e−4 | 22.9150 | 1.0000e−4 | 3.2130e−4 | 16.3087 |
| RGA [23] | −0.9506 | 3.0842e−3 | 7.7524e−5 | −1.8803e−4 | 22.9906 | 1.0027e−4 | 3.2900e−2 | 16.2746 |

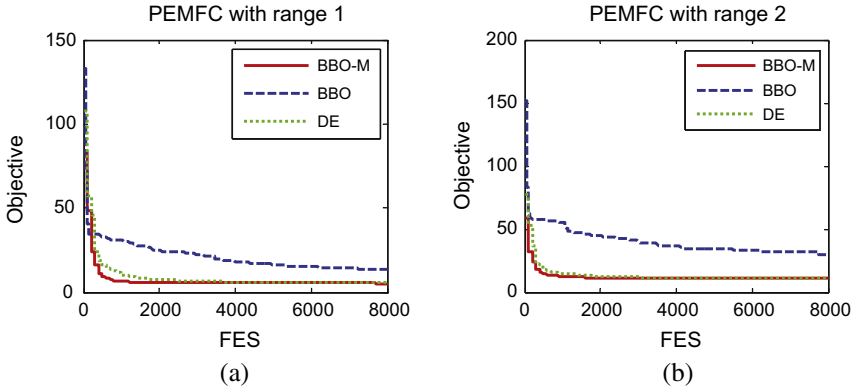


**Fig. 13.** (a) Convergence graphs of PEMFC with range 1. (b) Convergence graphs of PEMFC with range 2.

**Table 13**
Mean errors for four cell models.

| Method | BBO-M (%) | BBO (%) | DE (%) |
|---|---|---|---|
| Double diode solar cell | 0.96482 | 3.75044 | 0.97778 |
| Single diode solar cell | 0.72544 | 2.41017 | 0.81221 |
| PEMFC with range 1 | 1.65011 | 1.71560 | 1.70511 |
| PEMFC with range 2 | 2.52067 | 2.53563 | 2.53963 |

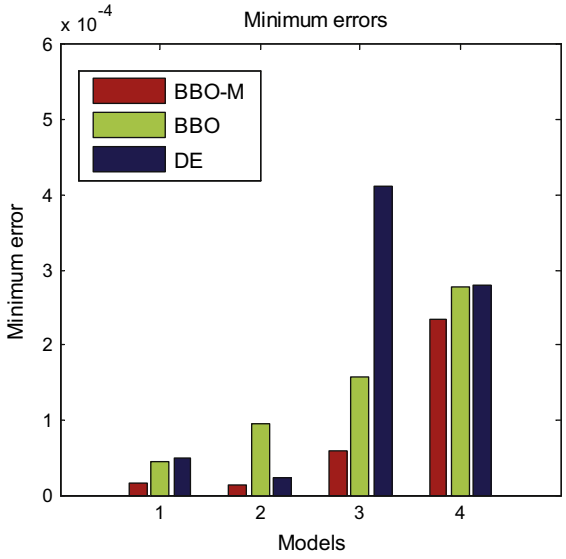


**Fig. 14.** Minimum errors in different models. (1) Double diode solar cell. (2) Single diode solar cell. (3) PEMFC with range 1. (4) PEMFC with range 2.

performance of the actual PEMFC system. The convergence of the algorithms for the PEMFC model with two parameter ranges are illustrated in Fig. 13. It is evident that BBO-M outperforms other approaches not only in finding smaller values of the objective function, but also in the convergence speed.

### 5.3. Error analysis

From the experiment results and the analysis, it can be concluded that by using BBO-M for parameter estimation of solar cell and PEM fuel cell models, the fitness $F_{min}$ decreases significantly. To further examine the performance of BBO-M, the error analysis of BBO-M, BBO, DE is conducted. The parameters obtained by the three algorithms are used to calculate the errors.

$$error = \frac{measured - calculated}{measured} \tag{28}$$

Table 13 shows the mean errors of the three algorithms in different cell models. It is obvious that the parameters found by BBO-M are closer to cell models than BBO, but similar to DE algorithm. Fig. 14 describes the minimum errors of the three methods. From these bar charts, it is clear that BBO-M is distinctively better than BBO and DE in producing the minimum errors in two kinds of cell models.

## 6. Conclusions

In this paper, a biogeography-based optimization algorithm with mutation strategies (BBO-M) has been proposed to estimate the parameters in the complex nonlinear solar cell and PEM fuel cell models. The BBO-M uses the frame of basic BBO algorithm, and incorporates the mutation strategies to increase the possibility of generating a new solution with better quality and controls the diversity of generations. In the numerical benchmark experiments, it is shown that BBO-M can effectively find better solutions than basic BBO and other four commonly used methods. Further, the BBO-M is applied to parameter estimation problems for solar cell and PEM fuel cell models. For solar cell models, the estimation results of double and single models show that BBO-M gives comparable performance to other reported results and basic BBO. For identification of PEMFC model with two different ranges, the experimental results demonstrate that the BBO-M has better searching ability and convergence speed. This paper shows that the BBO-M is a feasible and promising optimization algorithm in identifying the parameters of both solar cell and PEM fuel cell models.

## Acknowledgments

This work is supported by the National Natural Science Foundation of China (61273040), Shanghai Rising-Star Program (12QA1401100), and the project of Shanghai Municipal Education Commission (12YZ020).

## References

[1] Hanane H, Jamel G, Ahmed C. A real time fuzzy logic power management strategy for a fuel cell vehicle. Energy Convers Manage 2014;80:63–70.
[2] Giuseppe MT, Cristina V. Simulation tool for energy management of photovoltaic systems in electric vehicles. Energy Convers Manage 2014;78:851–61.
[3] Farivar F, Majid V, Omid R, Marc AR. Intelligent optimization to integrate a plug-in hybrid electric vehicle smart parking lot with renewable energy resources and enhance grid characteristics. Energy Convers Manage 2014;77:250–61.
[4] Berrazouane S, Mohammedi K. Parameter optimization via cuckoo optimization algorithm of fuzzy controller for energy management of a hybrid power system. Energy Convers Manage 2014;78:652–60.
[5] Maher AR, Haroun AK. Modeling optimizes PEM fuel cell performance using three-dimensional multi-phase computational fluid dynamics model. Energy Convers Manage 2007;48:3102–19.
[6] Caux S, Hankache W, Fadel M, Hissel D. PEM fuel cell model suitable for energy optimization purposes. Energy Convers Manage 2010;51:320–8.
[7] Biyikoglu A. Review of proton exchange membrane fuel cell models. Int J Hydrogen Energy 2005;30:1181–212.
[8] Ishaque K, Salam Z, Mekhilef S, Shamsudin A. Parameter extraction of solar photovoltaic modules using penalty-based differential evolution. Appl Energy 2012;99:297–308.
[9] Alexis DV, Aleksandra S, Viorel B. Modelling of solar cells with down-conversion of high energy photons, anti-reflection coatings and light trapping. Energy Convers Manage 2009;50:328–36.
[10] Amrouche B, Guessoum A, Belhamel M. A simple behavioural model for solar module electric characteristics based on the first order system step response for MPPT study and comparison. Appl Energy 2012;91:395–404.
[11] Orioli A, Di GA. A procedure to calculate the five-parameter model of crystalline silicon photovoltaic modules on the basis of the tabular performance data. Appl Energy 2013;102:1160–77.
[12] Sandrolini L, Artioli M, Reggiani U. Numerical method for the extraction of photovoltaic module double-diode model parameters through cluster analysis. Appl Energy 2010;87:442–51.
[13] Khan MJ, Iqbal MT. Modelling and analysis of electrochemical, thermal, and recetant flow dynamics for a PEM fuel cell system. Fuel Cells 2005;5:463–75.
[14] Easwarakhanthan T, Bottin J, Bouhouch I, Boutrit C. Nonlinear minimization algorithm for determine the solar cell parameters with microcomputers. Solar Energy 1986;4:1–12.
[15] Chan DSH, Phillips JR, Phang JCH. Comparative study of extraction methods for solar cell model parameters. Solid-State Electron 1986;29:329–37.
[16] Jian A, Kapoor A. Exact analytical solutions of the parameters of real solar cells using Lambert W-function. Solar Energy Mater Solar Cells 2004;81:269–77.
[17] Chegaar M, Nehaoua N, Bouhemadou A. Organic and inorganic solar cells parameters evaluation from single ICV plot. Energy Convers Manage 2008;49:1376–9.
[18] Saleem H, Karmalkar S. An analytical method to extract the physical parameters of a solar cell from four points on the illuminated J–V curve. IEEE Electron Dev Lett 2009;30:349–52.
[19] Yao X, Xu Y. Recent advances in evolutionary computation. J Comput Sci Technol 2006;21:1–18.
[20] AlRashidi MR, AlHajri MF, El-Naggar KM, Al- Othman AK. A new estimation approach for determining the *I–V* characteristics of solar cells. Solar Energy 2011;85:1543–50.

[21] Zhang L, Wang N. An adaptive RNA genetic algorithm for modeling of proton exchange membrane fuel cells. Int J Hydrogen Energy 2013;38:219–28.
[22] Mo ZJ, Zhu XJ, Wei LY, Cao GY. Parameter optimization for a PEMFC model with a hybrid genetic algorithm. Int J Energy Res 2006;30:585–97.
[23] Ohenoja M, Leiviska K. Validation of genetic algorithm results in a fuel cell model. Int J Hydrogen Energy 2010;35:12618–25.
[24] El-Naggar KM, AlRashidi MR, AlHajri MF, Al-Othman AK. Simulated annealing algorithm for photovoltaic parameters identification. Solar Energy 2012;86:266–74.
[25] Outeiro MT, Chibante R, Carvalho AS, de-Almeida AT. A new parameter extraction method for accurate modeling of PEM fuel cells. Int J Energy Res 2009;33:978–88.
[26] Huang W, Jiang C, Xue LY, Song DY. Extracting solar cell model parameters based on chaos particle swarm algorithm. In: IEEE World Congress on Electric Information and Control Engineering (ICEICE 2011); 2011. p. 398–402.
[27] Li X, Yan Q, Yu DT. PEMFC model parameter optimization based on a hybrid PSO algorithm. J Comput Inform Syst 2011;7:479–86.
[28] Askarzadeh A, Rezazadeh A. Optimization of PEMFC model parameters with a modified particle swarm optimization. Int J Energy Res 2011;35:1258–65.
[29] Sedighizadeh M, Rezazadeh A, Khoddam M, Zarean N. Parameter optimization for a PEMFC model with particle swarm optimization. Int J Eng Appl Sci 2011;3:102–8.
[30] Chakraborty UK, Abbott TE, Das SK. PEM fuel cell modeling using differential evolution. Energy 2012;40:387–99.
[31] Jiang LL, Maskell DL, Patra JC. Parameter estimation of solar cells and modules using an improved adaptive differential evolution algorithm. Appl Energy 2013;112:185–93.
[32] Bhagavatula YS, Bhagavatula MT, Dhathathreyan KS. Application of artificial neural network in performance prediction of PEM fuel cell. Int J Energy Res 2012;36:1215–25.
[33] Engin K, Mutlu B, Metin C. Neural network based solar cell model. Energy Convers Manage 2006;47:1159–78.
[34] Askarzadeh A, Rezazadeh A. A new heuristic optimization algorithm for modeling of proton exchange membrane fuel cell: bird mating optimizer. Int J Energy Res 2013;37:1196–204.
[35] Askarzadeh A. Parameter estimation of fuel cell polarization curve using BMO algorithm. Int J Hydrogen Energy 2013;38:15405–13.
[36] Dai CH, Chen WR, Cheng ZL, Li Q, Jiang ZL, Jia JB. Seeker optimization algorithm for global optimization: a case study on optimal modelling of proton exchange membrane fuel cell (PEMFC). Int J Electr Power Energy Syst 2011;33:369–76.
[37] AlHajri MF, El-Naggar KM, AlRashidi MR, Al-Othman AK. Optimal extraction of solar cell parameters using pattern search. Renew Energy 2012;44:238–45.
[38] Askarzadeh A, Rezazadeh A. Artificial bee swarm optimization algorithm for parameters identification of solar cell models. Appl Energy 2013;102:943–9.
[39] Simon D. Biogeography-based optimization. IEEE Trans Evol Comput 2008;12:702–13.
[40] Yao X, Liu Y, Liang KH, Lin GM. Fast evolutionary algorithms. Adv Evol Comput: Nat Comput Ser 2003:45–94.
[41] Yao X, Liu Y, Lin GM. Evolutionary programming made faster. IEEE Trans Evol Comput 1999;3:82–102.
[42] Hadidi A, Nazari A. Design and economic optimization of shell-and-tube heat exchangers using biogeography-based (BBO) algorithm. Appl Thermal Eng 2013;51:1263–72.
[43] Rajasomashekar S, Aravindhababu P. Biogeography based optimization technique for best compromise solution of economic emission dispatch. Swarm Evol Comput 2012;7:47–57.
[44] Xu ZD, Mo HW, Xu ZJ, Zhang JQ. Multi-objective biogeography-based optimization algorithm for the control of robotic manipulator. Adv Mater Res 2013;659:59–63.
[45] Rahmati SHA, Zandieh M. A new biogeography-based optimization (BBO) algorithm for the flexible job shop scheduling problem. Int J Adv Manufact Technol 2012;58:1115–29.
[46] Ammu PK, Sivakumar KC, Rejimoan R. Biogeography-based optimization – a survey. Int J Electron Comput Sci Eng 2013;2:154–60.
[47] May RM. Simple mathematical models with very complicated dynamics. Nature 1976;261:459–67.
[48] Storn R, Price K. Differential evolution – a simple and efficient adaptive scheme for global optimization over continuous spaces. Int comput sci instit, Berkeley, CA, Tech rep TR-95-012; 1995.
[49] Omran MGH, Mahdavi M. Global-best harmony search. Appl Math Comput 2008;198:643–56.
[50] Eberhart RC, Shi YH. Comparing inertia weights and constriction fac tors in particle swarm optimization. In: Proceedings of the IEEE conference on evolutionary computation, ICEC; 2000. p. 84–8.
[51] The Genetic Algorithm Toolbox for MATLAB was developed at the Department of Automatic Control and Systems Engineering of The University of Sheffield. <http://www.acse.dept.shef.ac.uk/cgi-bin/gatbx-download>.
[52] Wolf M, Noel GT, Stirm RJ. Investigation of the double exponential in the current–voltage characteristics of silicon solar cells. IEEE Trans Electron Dev 1977;ED-24:419–28.
[53] Gow JA, Manning CD. Development of a photovoltaic array model for use in power-electronics simulation studies. IEE Proc Electric Power Appl 1999;146:193–200.
[54] Mann RF, Amphlett JC, Hooper MAI, Jensen HM, Peppley BA, Roberge PR. Development and application of a generalized steady-state electrochemical model for a PEM fuel cell. J Power Sources 2000;86:173–80.